Nuclear magnetic resonance force microscopy with a microwire rf source

M. Poggio[a)]
IBM Research Division, Almaden Research Center, 650 Harry Rd., San Jose, California 95120 and Center for Probing the Nanoscale, Stanford University, 476 Lomita Hall, Stanford, California 94305

C. L. Degen, C. T. Rettner, H. J. Mamin, and D. Rugar
IBM Research Division, Almaden Research Center, 650 Harry Rd., San Jose, California 95120

(Received 3 May 2007; accepted 5 June 2007; published online 26 June 2007)

The authors use a 1.0 μm wide patterned Cu wire with an integrated nanomagnetic tip to measure the statistical nuclear polarization of ^{19}F in CaF_2 by magnetic resonance force microscopy. With less than 350 μW of dissipated power, the authors achieve rf magnetic fields over 4 mT at 115 MHz for a sample positioned within 100 nm of the "microwire" rf source. A 200 nm diameter FeCo tip integrated onto the wire produces field gradients greater than 10^5 T/m at the same position. The large rf fields from the broadband microwire enable long rotating-frame spin lifetimes of up to 15 s at 4 K. © *2007 American Institute of Physics*. [DOI: 10.1063/1.2752536]

The proposal of magnetic resonance force microscopy[1] (MRFM) and its subsequent realization[2] combine the physics of magnetic resonance imaging with the techniques of scanning probe microscopy. Recently, this marriage has led to the demonstration of nuclear spin imaging with a spatial resolution of 90 nm.[3] In order to eventually image on the scale of single nuclear spins, the force sensitivity of the measurement must be improved by roughly three orders of magnitude. Such an improvement will only be achieved if the dimensions of some key components are scaled down to more closely match the nanometer and sub-nanometer length scales of single spin physics. The most recent advances in sensitivity were the result of an increase in the magnetic field gradient provided by the scanning magnetic tip. Here, we discuss MRFM measurements done with a "microwire" rf source and an integrated nanomagnetic tip meant to further scale down the measurement apparatus. The reduced heat dissipation of this compact geometry allows us to simultaneously access temperatures under 300 mK and rf magnetic field amplitudes above 4 mT—fields large enough to produce remarkably long rotating-frame nuclear spin lifetimes.

We measure the statistical polarization[4] of ^{19}F spins in a CaF_2 crystal using a technique known as adiabatic rapid passage.[5] In a fixed magnetic field $\mathbf{B}_0$, we sweep the frequency ν_{rf} of a transverse rf magnetic field $\mathbf{B}_1$ through the nuclear resonance condition, $\nu_{rf}=(\gamma/2\pi)B_0$, where γ is the gyromagnetic ratio of ^{19}F. If done slowly enough, i.e., if the adiabatic condition $\partial\nu_{rf}/\partial t \ll (\gamma^2/2\pi)B_1^2$ is met, then the sweep induces nuclear spin inversions along the $\mathbf{B}_0$ direction. We then detect these inversions using a magnetic tip and an ultrasensitive cantilever as a force detector.

The force detection apparatus, shown in Fig. 1(b), uses a sample-on-cantilever configuration. The single crystal Si cantilever is 120 μm long, 3 μm wide, and 0.1 μm thick and includes a 15 μm long, 2 μm thick mass on its end.[6] The cantilever's mass-loaded geometry suppresses the motion of flexural modes above the fundamental frequency.[7,8] $A\sim 50$ μm^3 particle of CaF_2 crystal glued to the end of the lever serves as the sample. A thin layer of Si/Au (10/30 nm), with Si as an adhesion layer, is evaporated onto the end of the sample to screen electrostatic fields. At $T=4.2$ K the sample-loaded cantilever has a resonant frequency $\nu_c=2.6$ kHz and an intrinsic quality factor $Q_0=44\,000$. The oscillator's spring constant is determined to be $k=86$ μN/m through measurements of its thermal noise spectrum at several different base temperatures. The cantilever is mounted in a vacuum chamber (pressure $<1\times10^{-6}$ torr) at the bottom of a dilution refrigerator, which is isolated from environmental vibrations. The motion of the lever is detected using laser light focused onto a 10 μm wide paddle near the mass-loaded end and reflected back into an optical fiber interferometer.[9] 100 nW of light are incident on the paddle from a temperature-tuned 1550 nm distributed feedback laser diode.[10] We damp the cantilever using feedback to a quality factor of $Q=250$ in order to increase the bandwidth of our force detection without sacrificing force sensitivity.[11]

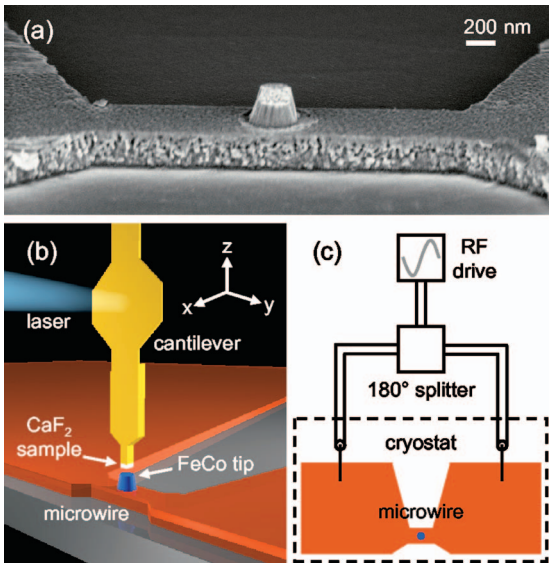

FIG. 1. (Color) (a) Scanning electron micrograph of the Cu microwire with integrated FeCo tip. (b) Representation of the experimental apparatus at the bottom of the cryostat (the relative scale of the components has been slightly altered). $\mathbf{B}_0$, the cantilever shaft, and the axis of the magnetic tip are aligned along $\hat{z}$. Current flows in the wire along $\hat{y}$, while at the position of the sample, the lever displacement and $\mathbf{B}_1$ are directed along $\hat{x}$. (c) Schematic diagram of the electrical connections to the microwire.

[a)]Electronics mail: poggio@stanford.edu

The key component of this experiment is the microwire rf source, which efficiently produces a strong rf magnetic field $\mathbf{B}_1$ for nuclear magnetic resonance. The Cu wire is 2.6 μm long, 1.0 μm wide, and 0.2 μm thick and is patterned atop a Si substrate, as shown in Fig. 1(a). The microwire bridges the gap between two 1 mm^2 pads and has a resistance of 0.35 Ω at $T=4.2$ K. In the middle of the microwire structure, deposited on its surface, is a 250 nm tall, 200 nm wide FeCo tip, in the shape of a truncated cone. This nanomagnetic tip provides the spatial magnetic field gradient required by the MRFM measurement.

We fabricate the microwire using lift-off, then we place the magnetic tip on the wire through a stencil-based process. First, a 450 nm layer of IBM KRS photoresist is patterned using electron-beam lithography on a prescribed wafer to define the copper wire. A Cr/Cu/Au (5/200/5 nm) film is then deposited via thermal evaporation and lifted off in hot solvent with ultrasonic agitation. To form the magnetic tip, a 500 nm thick film of polyimide is then spun onto the wafer and coated with a thin layer of evaporated Ti. A single hole is written above the wire, again with electron-beam lithography, in a resist covering the Ti. The Ti is then etched with a CF_4 plasma. Next, we etch the polyimide with an O_2 reactive ion etch through this hole to form a cavity. The resulting undercut Ti/polyimide bilayer structure forms a stencil mask over the wire onto which the magnetic film can be evaporated. This film consists of $Ti/Co_{30}Fe_{70}/Au$ (15/200/15 nm) deposited by e-beam evaporation. All the Au capping layers are meant to provide protection against oxidation. After final lift-off, the wafer is cleaved along the preexisting scribe in order to place the wire less than 50 μm from the edge of the chip. The structure's proximity to the edge ensures a clear optical path from the fiber interferometer to the cantilever paddle.

The overall geometry of the MRFM apparatus is shown in Fig. 1(b). During measurement, the sample at the end of the cantilever is situated less than 100 nm directly above the nanomagnetic tip. At such a small spacing, the magnetic tip provides fixed spatial field gradients in excess of 10^5 T/m. Less than 20 mA passing through the microwire (current density $\sim 10^7$ A/cm^2) produce rf B_1 fields larger than 4 mT (rotating field) at the position of the sample. Under these conditions, the heat dissipated by the wire is under 350 μW allowing the dilution refrigerator to reach temperatures below 300 mK. The rf current required to produce B_1 flows through the microwire from the pads on either side of it. These pads are each connected through short Cu leads to the center conductors of semirigid coaxial lines leading to the top of the cryostat. The two lines are differentially driven by a 180° splitter, which is in turn connected to the rf drive signal, as shown in Fig. 1(c). By matching the attenuation and delay caused by each coaxial line, this differential driving scheme results in a voltage node and a current antinode at the microwire. In this way, we maximize the rf magnetic field produced around the microwire while minimizing unwanted electric fields, which could cause spurious excitation of our cantilever. Note that since the wire is not frequency specific it has the flexibility of being a broadband source of rf magnetic field. In the present experiment, the upper frequency limit is about 200 MHz due to the inductance of the wire leads.

In typical MRFM measurements of the ^{19}F spin polarization by adiabatic rapid passage, we drive the microwire with the frequency-sweep waveform represented in the inset to Fig. 2. In these experiments we use a center frequency $\nu_{rf}=114.7$ MHz and a peak-to-peak frequency deviation $\Delta\nu=1.4$ MHz. A superconducting magnet provides the resonant field for ^{19}F of $B_0 \simeq 2.9$ T. By generating an rf magnetic field whose frequency is swept through the ^{19}F resonance twice every cantilever period T_c, we drive longitudinal nuclear spin flips in the sample at the lever's resonance frequency. Since the sample is mounted on the end of the cantilever, in the presence of a large enough magnetic field gradient, the spin flips produce a force that drives the lever. By measuring the amplitude of the cantilever's oscillation on resonance we determine the longitudinal component of net spin polarization. In our case, this polarization is due to the naturally occurring $\sqrt{N}$ statistical component. The cantilever displacement induced by adiabatic passages is shown in the vibrational spectrum plotted in Fig. 2. The narrow band spin signal, whose spectral width is inversely proportional to the rotating-frame spin lifetime τ_m, sits atop a much broader peak generated by the lever's natural thermal vibrations.

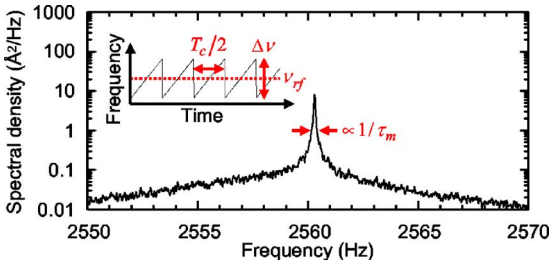

FIG. 2. (Color online) Power spectral density of cantilever displacement during adiabatic rapid passage of a statistical polarization of ^{19}F spins. The inset represents the frequency sweep of $\mathbf{B}_1$ that induces the passages.

To measure the magnitude of B_1, which the microwire produces in the sample, a different rf protocol, shown schematically in Fig. 3(a), is used. We sweep the frequency ν_{rf} of B_1 through resonance twice per cantilever period, as discussed previously, and intersperse the frequency sweeps with occasional resonant pulses of variable width τ_p, spaced by T_p. Here we use $T_p=196$ ms or $502\times T_c$. Given a fixed amplitude B_1, as we increase τ_p, the resonant pulses induce spins to nutate with an increasing angle. If the pulse spacing is much less than the rotating-frame spin lifetime, $T_p \ll \tau_m$, nutations produced by the pulses modulate the force signal generated by the adiabatic passages. When $\tau_p=\pi/(\gamma B_1)$, i.e., the pulse width and amplitude is equivalent to π radians of nutation, each pulse reverses the sign of the force signal. This modulation results in sidebands appearing in the frequency spectrum of the cantilever displacement signal spaced by $1/(2T_p)$ from the lever resonance at ν_c. The signal power formerly in the central peak shifts to the sidebands and back again depending on the rf pulse width τ_p, as shown in Figs. 3(b)–3(d). By feeding the displacement signal into a narrow band lock-in amplifier referenced to ν_c, we measure the power at ν_c as a function of τ_p and observe the Rabi oscillations plotted in Fig. 3(e). From the period of these oscillations we extract the pulse width required for 2π radians of nutation, $\tau_{2\pi}$. Using the relation $B_1=2\pi/(\gamma\tau_{2\pi})$, we determine the magnitude of B_1 produced by the microwire at the sample position. Aquiring data similar to those shown in Fig. 3(e) taken at different rf drive amplitudes, we calibrate the magnitude of B_1 at the sample position corresponding to a given rf drive.

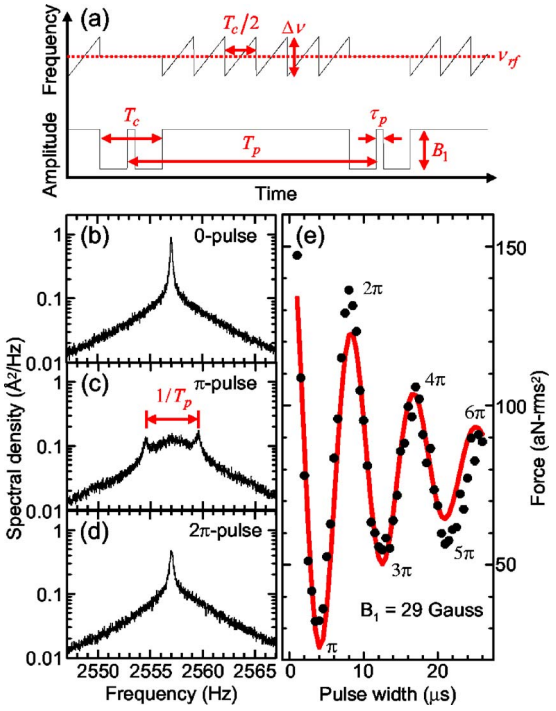

FIG. 3. (Color online) (a) rf pulse protocol for the spin nutation experiment. The resulting power spectral density of cantilever displacement with pulse widths τ_p equivalent to (b) 0, (c) π, and (d) 2π radians of nutation. (e) The corresponding force signal is measured through a narrow band lock-in amplifier and plotted in points as a function of pulse width τ_p. A B_1 amplitude can be extracted from a decaying cosinusoidal fit of the Rabi oscillations shown in red.

In order to investigate the dependence of τ_m for ^{19}F nuclei in CaF_2 as a function of increasing rf magnetic field B_1, we employ the adiabatic sweep waveform without the interspersed pulses, shown in the inset to Fig. 2. As plotted in Fig. 4, τ_m strongly increases with increasing B_1 amplitude up to a saturation around $\tau_m=15$ s at $B_1=3$ mT. Previous low-temperature nuclear MRFM experiments were done with $B_1<2$ mT due to the large heat dissipation caused by the larger than 200 μm diameter coils used as rf sources.[3] These conditions resulted in $\tau_m<500$ ms. In this low B_1 regime, rotating-frame lifetimes are often very short due to either violation of the adiabatic condition,[12] spin-spin interactions, or spin relaxation caused by the thermal vibration of higher order cantilever modes in the strong field gradients provided by the nanomagnetic tip.[7,8]

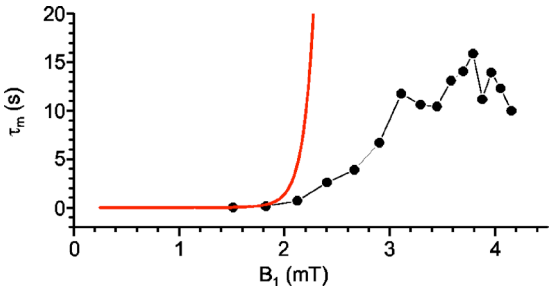

FIG. 4. (Color online) Plot of the τ_m as a function of B_1 in the sample at $T=4.2$ K. Red line corresponds to the limit set on τ_m by the adiabatic condition and is calculated using numerical integration of the Bloch equations for repetitive linear frequency sweeps of ν_{rf} through resonance (Ref. 13).

In addition to accessing a regime of long τ_m, the small amount of heat dissipated by the microwire—even for large B_1 amplitudes—is the fundamental advance presented here. Previous nuclear MRFM experiments were done with a hand-wound coil larger than 200 μm in diameter as a rf source; the coil produced less than 2 mT at the sample with more than 200 mW of dissipated heat. In contrast, since our microwire can be less than 100 nm from the sample, it produces more than 4 mT with less than 350 μW of dissipated heat.

The authors thank M. Hart and M. Farinelli for assistance with magnetic tip fabrication. The authors acknowledge support from the DARPA QuIST program administered through the Army Research Office, the NSF-funded Center for Probing the Nanoscale (CPN) at Stanford University, and the Swiss National Science Foundation.

[1] J. A. Sidles, Phys. Rev. Lett. **68**, 1124 (1992).
[2] D. Rugar, C. S. Yannoni, and J. A. Sidles, Nature (London) **360**, 563 (1992).
[3] H. J. Mamin, M. Poggio, C. L. Degen, and D. Rugar, Nat. Nanotechnol. **2**, 301 (2007).
[4] H. J. Mamin, R. Budakian, B. W. Chui, and D. Rugar, Phys. Rev. Lett. **91**, 207604 (2003).
[5] C. P. Slichter, *Principles of Magnetic Resonance*, 3rd ed. (Springer, New York, 1990), Chaps. 2 and 6, pp. 11–64 and 219–246.
[6] B. W. Chui, Y. Hishinuma, R. Budakian, H. J. Mamin, T. W. Kenny, and D. Rugar, *Technical Digest of the 12th International Conference on Solid-State Sensors and Actuators (Transducers '03)* (IEEE, Boston, MA, 2003), p. 1120.
[7] D. Mozyrsky, I. Martin, D. Pelekhov, and P. C. Hammel, Appl. Phys. Lett. **82**, 1278 (2002).
[8] G. P. Berman, V. N. Gorshkov, D. Rugar, and V. I. Tsifrinovich, Phys. Rev. B **68**, 094402 (2003).
[9] D. Rugar, H. J. Mamin, and P. Guethner, Appl. Phys. Lett. **55**, 2588 (1989).
[10] K. J. Bruland, J. L. Garbini, W. M. Dougherty, S. H. Chao, S. E. Jensen, and J. A. Sidles, Rev. Sci. Instrum. **70**, 3542 (1999).
[11] J. L. Garbini, K. J. Bruland, W. M. Dougherty, and J. A. Sidles, J. Appl. Phys. **80**, 1951 (1996); K. J. Bruland, J. L. Garbini, W. M. Dougherty, and J. A. Sidles, *ibid.* **80**, 1959 (1996).
[12] C. W. Miller and J. T. Markert, Phys. Rev. B **72**, 224402 (2005).
[13] J. Baum, R. Tycko, and A. Pines, Phys. Rev. A **32**, 3435 (1985).